Biosensors and Bioelectronics 159 (2020) 112186

Contents lists available at ScienceDirect

Biosensors and Bioelectronics

journal homepage: http://www.elsevier.com/locate/bios

Enhancement of cortisol measurement sensitivity by laser illumination for AlGaN/GaN transistor biosensor

Kyoungmin Woo [a], Wonkyu Kang [a], Kyungmin Lee [a], Pilwoo Lee [a], Yoonjae Kim [a], Tae-Sik Yoon [b], Chu-Young Cho [c], Kyung-Ho Park [c], Min-Woo Ha [d,**], Hyun Ho Lee [a,*]

[a] Department of Chemical Engineering, Myongji University, Yongin, 17058, Republic of Korea
[b] Department of Material Science and Engineering, Myongji University, Yongin, 17058, Republic of Korea
[c] Korea Advanced Nano Fab Center (KANC), Suwon, 16229, Republic of Korea
[d] Department of Electrical Engineering, Myongji University, Yongin, 17058, Republic of Korea

ARTICLE INFO

Keywords:
AlGaN/GaN
HEMT
Cortisol
Biosensor
Laser illumination

ABSTRACT

In this study, high electron mobility transistor (HEMT) device was used as an immuno biosensor to measure concentration of a stress hormone, cortisol, by using selective binding on cortisol monoclonal antibody (c-Mab). Also, the HEMT sensor was enhanced in its sensitivity through light illumination to generate photocurrent. The optical pumping could assist the biosensor to discriminate more detailed change, which could result in an increment of limit of detection (LOD) to 1.0 pM cortisol level. It was the lowest level of detection with semiconductor device-based cortisol biosensors and the enhancement of surface potential sensitivity was induced by laser light (532 nm). Output current amplificated by photocurrent was higher than dark original current at about 3.39% when gate voltage is applied with −3 V. Since the device could be applied to not only standard cortisol solution but also real human salivary sample, it is expected to apply for *in vitro* direct diagnosis of point-of-care test (POCT).

1. Introduction

Nowadays, psychological chronic stress is one of social key issues in modern society, where increased depression patients and corresponding suicides were originated from. Many literatures on depression and attempted suicide frequently have regarded both behaviors as reactions to life stress, as exemplified in the concept of reactive depression. (Arya et al., 2010a, 2010b; Kim et al., 2015). Moreover, for long-term stress monitoring and management, utilization of objective index could be digitized to understand both syndromes instinctively. In this condition, many researches have been paying attentions to correlation between stress rate and stress hormone, cortisol, concentration in body. They also have attempted to apply concentrations as an indicator of the stress rate (Domes et al., 2019).

The cortisol is a steroid hormone secreted from an adrenal cortex on kidney. There are diverse methods to extract real human cortisol sample from blood, urine and salivary (Kim et al., 2017; Jung et al., 2018). Among them, the salivary cortisol is good choice in terms of noninvasive and rapid acquiring method. Also, it is routinely used as a biomarker of psychological stress and related mental or physical diseases. Most studies have considered salivary cortisol levels as a reliable measurement marker of hypothalamus-pituitary-adrenal axis (HPAA) adaptation to stress (Hellhammer et al., 2009). Viewed in this way, several teams easily could apply this study to detect salivary cortisol. They could accomplish reduced graphene oxide (rGO) as electrochemical sensing platform and accomplish to 10 pM, 27.6 pM for limit of detection (LOD), respectively. (Kim et al., 2015, 2017). Furthermore, one study has been attempted to a wearable organic electrochemical device with a noninvasive method for cortisol (Parlak et al., 2018).

The cortisol concentration can be measured easily by ELISA (Enzyme-linked immunosorbent assay) or radioimmunoassay (RIA) (Sun et al., 2008). However, they could be unsuitable sometimes since they require lengthy measurement period for normal personnel to require massive equipment and complicated preconditioning process. Therefore, a biosensor should have advantages of easy access, fewer or more compact equipment, accurate and sensitive detection in a few

* Corresponding author. Tel.: 82 31 330 6392; fax: 82 31 330 6957.
** Corresponding author.
E-mail addresses: isobar@mju.ac.kr (M.-W. Ha), hyunho@mju.ac.kr (H.H. Lee).

https://doi.org/10.1016/j.bios.2020.112186
Received 10 February 2020; Received in revised form 30 March 2020; Accepted 1 April 2020
Available online 12 April 2020

different concentrations.

To meet these requirements, various biosensing systems have been rapidly developed such as cyclic voltammetry (C–V) (Kim et al., 2015) or impedance spectroscopy (Kim et al., 2016), and surface plasmon resonance (SPR) (Jeon et al., 2018; Jo et al., 2020). Among many sensors, field effect transistor (FET)-based biosensor (Chen et al., 2011; Stern et al., 2007) have been demonstrated to possess exceptionally simplicity and outstanding performance while conjugated with the advanced nanotechnology (Shen et al., 2014). It has good advantages of satisfying high sensitivity, low LOD, easy signal reading, and small size chip without label (Sarangadharan et al., 2018; Shen et al., 2014; Choi et al., 2012). The FET-based biosensors could have detected bio-molecules by tracing a change in the current caused by specific effect arising from the bio-molecules (Choi et al., 2012). One of various FETs, aluminum gallium nitride/gallium nitride (AlGaN/GaN) high-electron-mobility transistor (HEMT) biosensors have been attempted several times (Steinhoff et al., 2003). The AlGaN/GaN HEMTs have unique characteristics of high carrier density and high mobility at two-dimensional electron gas (2DEG) (Ambacher et al., 1999). The AlGaN/GaN heterostructure with wurzite crystal structure has strong spontaneous and piezoelectric polarization at the interface between AlGaN and GaN. The Fermi level is upper than the conduction band at the interface which is 2DEG as the conductive channel in transistor. Variation of the channel current, or 2DEG density can be explained by compensation of the polarization-induced bound surface charge by the interaction with the polar molecules in the liquids. (Neuberger et al., 2001; Yang et al., 2017).

Because this effect fully increased possibility to be used as sensor, many researches in various fields have grafted the HEMT onto gas-sensor and biosensor using various structures and receptor methods. Very recently, gate-pulsed measurement strategy was introduced to evoke more interests and potentials to be adopted as biosensor for the detection of protein, DNA, and hormones (Yang et al., 2017; Varghese et al., 2019).

The AlGaN/GaN HEMT has been known to provide photocurrent due to generated carriers under laser exposure by detrapping mechanism of electrical carriers. Actually, one research team demonstrated this study with AlGaN/GaN HEMT with 671 nm, 532 nm, 447 nm laser exposure and finally calculated increasing rate of sheet carrier and detrapping activation energy (Kang et al., 2015, 2016). Therefore, since the HEMT with a higher channel conductivity could show a better sensitivity as FET biosensor, it can be proposed that optical pumping of trapped charge or photocurrent is expected to enhance its sensitivity of biomolecule detection.

In this study, AlGaN/GaN HEMT was adopted for a cortisol FET biosensor. Here, cortisol capture could be progressed by antigen-antibody's immune-binding with a high selectivity, and cortisol detection could be verified by output curve saturation area as current decrease. Further, we suggest positive effect of photocurrent by detrapping traped electron induced by 532 nm green laser illumination to enhance sensitivity by decreasing its LOD. In addition, optical pumped-HEMT biosensor could be also applicable to real samples of human saliva.

2. Material and methods

2.1. Fabrication of AlGaN/GaN HEMT

We used 4-inch (0001) sapphire substrates, and AlGaN/GaN layers were grown using metal-organic chemical vapor deposition (MOCVD). The epitaxial layers consisted of (from bottom to top) a 25 nm thick low temperature GaN nucleation, a 1 μm thick C-doped GaN buffer layer, a 1.5 μm thick unintentionally doped GaN, and a 28 nm thick i-$Al_{0.27}Ga_{0.73}N$ barrier layer (Pyo et al., 2018). The thick GaN buffer is suitable for high-voltage devices with a short drift length between source and drain. It was designed to enhance the depletion region in a vertical direction under large reverse bias. The sheet electron density was $10^{13}/cm^2$, and the electron mobility in the virgin AlGaN/GaN structure was 1900 cm^2/V, as measured using the Hall effect. The overall layout of the HEMT device was designed as extended gate (EG) format for a detection of liquid pH (Pyo et al., 2018). However, the EG structure was not used as sensing region in this study.

Samples were cleaned in an ultrasonic bath using a sequence of acetone, methanol, and isopropyl alcohol (IPA). Isolation structures were formed to isolate individual devices using an inductively coupled plasma (ICP) etch with Cl_2/BCl_3 etchant gases, forming 500 nm depth. Metal contacts were deposited using electron-beam evaporation (e-beam evaporation) and defined using lift-off process. Ohmic contacts at the cathode were formed by 830 °C RTA annealing for 1 min. Ti/Al/Ni/Au (20/100/25/50 nm) metal stack. For the formation of the Schottky barrier, contacts were patterned using optical lithography and the surface was cleaned using buffered oxide etchant (BOE) to remove the group-III oxides. Ni/Au (20/100 nm) stack was then deposited to form the Schottky contact.

The final size after completion of entire steps of the fabrication process was measured by optical microscopy (OM). The gate-drain length, gate length, gate-source length, and device width were 16 μm, 243 μm, 16 μm, and 227 μm, respectively.

2.2. Preparation of PDMS microfluidic systems

The microfluidic system platform was adopted on top of the HEMT sensor to ensure that all solutions could influence only on liquid accessible gate area specifically. Polydimethylsiloxane (PDMS) was chosen for the implementation of microfluidic system due to its transparency. The mold for PDMS microfluidic was cast by SU-8 2025 (Microchem, 2025), that was spin coated twice at 800 rpm for 65 s on bare silicon wafer. Then, the SU-8 photoresist film was soft baked for 5 min at 65 °C and for 15 min at 90 °C in a sequence. Then, SU-8 2025 was patterned by 35 s exposure time of UV light with mask aligner (MDA-8000, Midas Co, Korea) followed by post exposure bake (PEB) for 5 min at 65 °C and 25 min at 90 °C, respectively. Immediately after the exposure, SU-8 was developed gently with SU-8 developer (Microchem). The SU-8 mold is covered with PDMS solution, which is blended with pre-polymer of PDMS sylgard 184A (Dow corning Co) and cross linker sylgard 184B solution as 10:1 ratio under vacuum to remove the resident bubbles. Finally, the poured PDMS solution on the SU-8 2025 mold could turn into jelly solid after annealing at 70 °C overnight.

The PDMS microfluidic part could be chemically attached on AlGaN/GaN HEMT by chemical bonding formation. Thereby, solution can pass through channel or piping without any leakage. It was accomplished with GPTMS ((3-Glycidyloxypropyl) trimethoxysilane, sigma-aldrich)-APTES ((3-Aminopropyl) triethoxysilane, Sigma-Aldrich) chemical glue. First, both PDMS and HEMT surface were activated by UV/Ozone treatment for 10 min. Next, GPTMS and APTES 5 vol % solutions in ethanol (Sigma- Aldrich) were poured immediately on the UV/Ozone activated surface areas of PDMS and HEMT, respectively (Kim et al., 2012). After 30 min, two different surface could accomplish an epoxy-amine bond. The surfaces of PDMS and HEMT were cleaned with pure ethanol completely and aligned at each other after lightly brushing aside of residual ethanol without drying solvent. The aligned device with little ethanol was pressed hard to adhere perfectly to each other for 40 min at room temperature and in sequence, for 15 min at 60 °C.

2.3. Conjugation of c-Mab and cortisol measurement

Since thiol functional group (-SH) of 3,3′-dithiodipropionic acid di (N-hydroxysuccinimide ester) (DTSP, Sigma Aldrich) has selective reaction toward gold, the DTSP can make link between gold thin film of gate electrode and cortisol monoclonal antibody (c-Mab, Abcam Co., 2 mg/mL) to build functionalized gate area as shown in Figure 1(b). First, 4 mg/mL DTSP in reagent plus dimethyl sulfoxide (DMSO, Sigma-Aldrich) was passed through the microfluidic system for three times

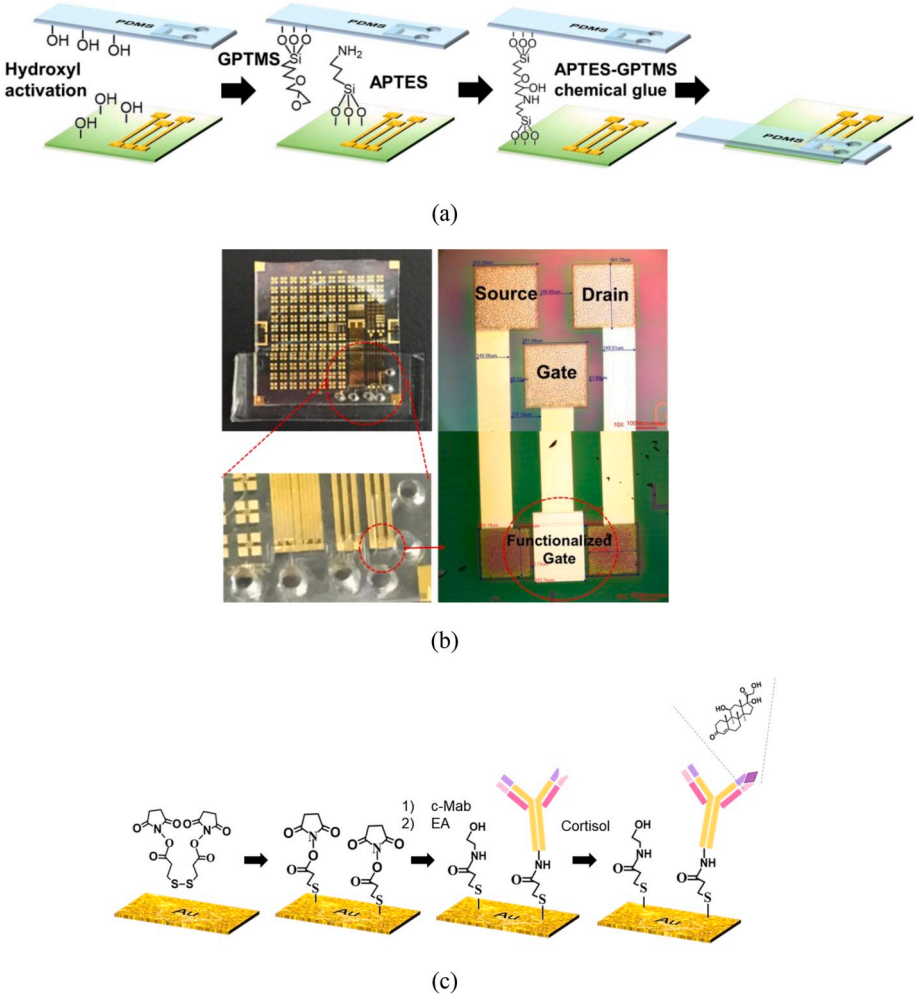

Fig. 1. (a) Scheme of APTES-GPTMS chemical glue process (b) OM image of AlGaN/GaN HEMT device including source, drain, gate and functionalized (right), PDMS microfluidic platform image on the device (left) (c) illustration of process of chemical treatment for Au gate functionalization to conjugate c-Mab and detect cortisol molecule.

and it was incubated for 2 h to finish the chemical linkage thoroughly. After that, c-Mab solution, which was diluted as 10 μg/mL in deionized (DI) water was also passed by the microchannel to immobilize the c-Mab probe for 2–4 h. The c-Mab immobilized area was labeled as functionalized gate area that was electronically connected with gate for applying gate voltage. Next, diluted cortisol solutions (Cerilliant Co., 1 mg/mL in methanol) ranging from 1 pM, 10 pM, 100 pM, and 1 nM were progressed and sequentially applied for 30–60 min in the same way. Ahead of the next step in all processes of experiment, DI water was similarly passed through the microchannel three times equally to rinse resident chemicals, and it was left for 5 min, respectively. In a case of cortisol detection from real human salivary sample, 100 mM ethanol amine (EA) in methanol was employed for 30 min for passivation to block non-specific protein binding and unwanted DTSP linking which was not reacted with the c-Mab. Since a lot of non-specific or unwanted proteins in salivary could link with DTSP linker in contrast with standard cortisol solution diluted as planned concentration in DI water, influencing result of measurement.

For real human cortisol salivary samples, the samples were centrifuged in vivaspin 10,000 having 30,000 molecular weight cut-off (MWCO) for 10 min at 3000 rpm to remove any solid contaminants. The filtered solution was collected in a separate micro-tube. Since the amount of cortisol secretion was known to be varied on sampling time of day, the real salivary samples were collected twice in same day after morning rise-up and before sleep at night. The highest concentration in the morning and the lowest concentration at night were expected in this study. Typically, average salivary cortisol concentration in human body system is 1–20 nM, having gap about 6–8 times between maximum and minimum (Arya et al., 2010b; Kim et al., 2017). In this study, HEMT's biosensor detection range was identified with 1 pM–1 nM. Therefore, for an experiment with salivary samples in guaranteed range, samples were required to be diluted about hundredfold with DI water. So, filtered salivary samples were diluted in 200 × , 100 × , 10 × solution. Therefore, measurements were progressed same as standard solution experiment method from low concentration (200 ×) to high concentration (1 × : original sample). To prove the chemical conjugation reaction on gate surface, FT-IR (Jasco 460, Japan) was used to analyze the functional groups of the DTSP and c-Mab. For analysis of UV–Vis spectrophotometer (Shimadzu UV-1601, Japan), absorbance mode was used.

Cortisol measurements were conducted with interpretation of the HEMT biosensor's transfer curve and output curve at saturation region by Agilent 4156C semiconductor parameter analyzer. In addition, light sources for optical pumping with 532 nm green laser and 623.8 nm red laser were employed below 1 mW power, which is a simple laser pointer for presentation purpose.

3. Results and discussion

3.1. Pristine HEMT and biosensor platform

Fig. 1(a) shows an illustration for procedure of the GPTMS-APTES chemical glue and fabricated PDMS microfluidic sensor platform on AlGaN/GaN HEMT. The PDMS can attach on glass substrate using UV/Ozone treatment for fabricating hydroxyl group. However, the gluing was accomplished not only with UV/Ozone activation but also any substrates to generate hydroxyl functional group (-OH) such as by typical plasma treatment. GPTMS and APTES can link generated hydroxyl group (-OH) on PDMS and glass substrate (Kim et al., 2012; Lee et al., 2019). UV/Ozone treatment was performed to activate the –OH groups on both PDMS and AlGaN/GaN HEMT. In ethanol solvent, –OH groups on PDMS was changed epoxy-terminated silane and –OH on HEMT substrate was induced amine-terminate silane and these two separate groups could combine easily due to chemical coupling by substitution reaction. We successfully constructed microfluidic system without any leakage as shown in Fig. S1.

Typically, the key issue of biosensors is the stability to guarantee low LOD which should be consistent at any time. The exact modification on surface at sensing area is critical. The Au have good property to selectively conjugate with thiol functional group (-SH) by self-assembled monolayers (SAMs) formation (Vericat et al., 2010). Also, a method to link gold (Au) metal surface and antibody was well known to be accomplished by DTSP's thiol group and amine group (Arya et al., 2010a, 2010b; Vasudev et al., 2013). In a word, this gold's advantage along with stability could lead that gold metal was selected as area of gate in HEMT. The Au gate with antibody conjugation with antibody was labeled as 'functionalized gate', which could affect in a sequence drain current decreasing or increasing, which determine sensor detection index. The process was illustrated in Fig. 1(c).

FT-IR spectra could demonstrate the change of the gold surface featured from DTSP alone and DTSP-antibody by substitution reaction between DTSP's NHS (N-hydroxylsuccinimide) ester group and antibody's primary amine group (-NH_2). Fig. S2 shows the measured FT-IR spectra of the functionalized Au gate in AlGaN/GaN HEMT. It was noted that the FT-IR spectra proved that the c-Mab probe selectively captured and detected the cortisol molecule (Jung et al., 2018).

The pristine AlGaN/GaN HEMTs were fabricated and their electrical characteristics were measured. As gate voltage and drain voltage was applied, carrier concentration between interface of AlGaN/GaN was changed, influencing the detection performance.

Figure 2(a)–(b) show the transfer and output characteristics of the pristine AlGaN/GaN HEMT. The measured threshold voltage (V_{TH}) was −4.4 V using extracting slope of squared drain current at drain-source voltage (V_{DS}) of 1 V. The cut-off region where V_{GS} was less than V_{TH} did not allow any current flow. The pristine device could have disparate linear and saturation regions from output characteristics when V_{GS} was swept from −3 to 1 V. The extracted on-resistance from the linear region were 404.5 and 98.6 Ohm-mm at V_{GS} of −3 and 0 V, respectively, under V_{DS} of 0.5 V. The forward current from the saturation region were 2.1 and 23.7 mA/mm at V_{GS} of −3 and 0 V, respectively, under V_{DS} of 5 V. The pristine device has low differential current and high on-resistance from the saturation region. Functionalized device using pristine AlGaN/GaN HEMT was fabricated with further DTSP chemical treatment and c-Mab coupling to accomplish biosensor.

Fig. 3 shows the measured output characteristics of the pristine device, DTSP treatment device, functionalized device coupling with c-Mab, and functionalized device after cortisol sensing. Since the HEMT biosensor was not open-gated format, it was not anticipated that drastic or intense measurement changes with respect to threshold voltage shift (ΔV_{TH}) could occur during sensing (Kokawa et al., 2006). However, even though the open-gate will be advantageous for the ΔV_{TH}, there can be a severe instability with the open-gated AlGaN/GaN sensor during the chemical conjugation step with biomarkers such as antibody,

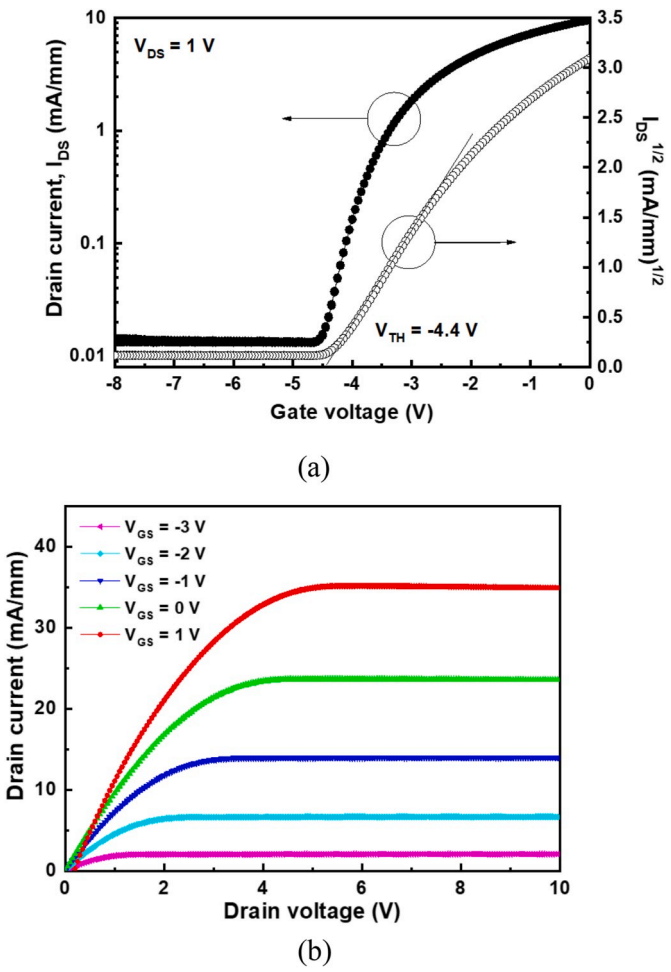

Fig. 2. I–V curves of (a) transfer and (b) output characteristics of the pristine AlGaN/GaN HEMT.

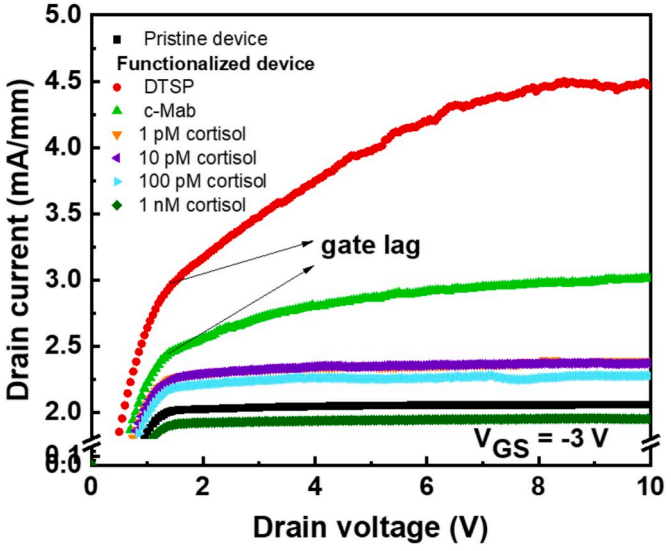

Fig. 3. Measured output characteristics of the pristine AlGaN/GaN HEMT and functionalized devices with DTSP, c-Mab, respectively. After the functionalization, cortisol detection was progressed with standard cortisol solution in DI water, whose concentrations were 1 pM, 10 pM, 100 pM, and 1 nM.

Therefore, gate electrode like Au layer in this study can be appropriate at the sacrifice of the sensing strategy. In addition, the Au surface has been widely developed as a suitable surface for biomolecule or biomarker conjugation (Kim et al., 2017).

The functionalized device detected standard cortisol solution with different concentrations of 1 pM, 10 pM, 100 pM, and 1 nM, respectively as shown in Fig. 3. To demonstrate a distinct detection, measurement strategy was progressed from the lowest (1 pM) to the highest concentration measurement (1 nM). The DTSP chemical treatment and c-Mab coupling functionalization and cortisol antigen-antibody binding sensing could change the forward drain current. The DTSP increased the output current from 2.04 to 3.98 mA/mm at V_{DS} of 5 V read voltage.

In a word, the device after DTSP chemical treatment on Au gate surface could obtain the highest drain current as shown in Fig. 3. However, coupling with c-Mab and cortisol sensing by antigen-antibody binding could result in decreases of the drain currents in regular sequence. Huq team also reported that DTSP treatment on gold gate surface increase the output current (Huq et al., 2016).

This sensing mechanism can be explained by gate surface charging and carrier concentration. The source-drain current is modulated by a Schottky type gate on the top of the 2DEG channel. The target material on the gate region could alter the accumulated charge, which eventually form bias and differ the 2DEG resistance. Finally, this detecting signal from gate surface could be amplified to source-drain current (Pearton et al., 2013). Therefore, surface charging is the key point to detection principle, which is a source of variation of current followed by carrier concentration (2DEG).

For the detection of 1 pM and 10 pM, it can be proposed that there were no enough differences in surface charging or carrier concentration. At the same time, it has been known that an electronic double layer on the gate metal of the 2DEG device would be formed (Yang et al., 2017). Once the cortisol is bound to its antibody tethered to the HEMT biosensor, the effective capacitance of gate dielectric will be changed to result in the voltage change on the gate electrode, sequentially changing of corresponding I_{DS}. Typically, there has been no report of high sensitivity with the AlGaN/GaN HEMT biosensor detecting a small molecule like cortisol (Varghese et al., 2019). In other word, large target molecules like proteins or cells, which could easily induce the effective capacitance change, could be detected substantially. In this study, it means that there was no effective difference in the formation of electronic double layers with both 1 pM and 10 pM. In same view, there is a report that exposure of AlGaN/GaN HEMT gate surface to the media including CHO–K1 and HEK293FT cells decreased the sheet carrier concentration between AlGaN and GaN (Cimalla et al., 2007).

As a point of view regarding to organic electron transport, the NHS (N-hydroxysuccinimide) ester group of the DTSP, which consists of an electron withdrawing group of succinimide, could be another source of carrier concentration change. Due to the electron withdrawing group of the DTSP molecule, Au surface would be relatively positive charged. Therefore, the positively charged surface could induce more two dimensional electron gas (2DEG), increasing forward source-drain current. In the same context, the gate-lag phenomenon was also presented in Fig. 3, of which property could be resulted from an influence of gate surface trap.

The HEMT surface charging has been discussed in various studies, which can be easily ensured by three phenomenon, that is, gate leakage current, V_{TH} instability in transfer curve, and gate lag in output curve (Lagger et al., 2012; Horio and Nakajima, 2010; Saito et al., 2005). The sensing tendency can different according to the device structure and eventually to the surface charges. A report about the association between gate surface charge of AlGaN/GaN HEMT and sensing tendency for Troponin I with two different type structure could be an instance. In the research, one type shows increasing current tendency, while another type shows decreasing current tendency although there are same target reagent, Troponin I and probe antibody (Lee et al., 2015; Yang et al., 2017). So, various studies have been reported by different probe or receptor materials with different detection tendency. The detections of C-reactive protein (CRP) and Troponin I were studied and reported with Au gate AlGaN/GaN HEMTs, respectively. In Lee's study, Au gate was functionalized by EDC-NHS self assembly monolayer (SAM) for coupling with the CRP-antibody. Output current was decreased after the SAM treatment and it was increased after conjugation of the CRP-antibody or probe molecule. Finally, there were output current decreases after antigen-antibody or CRP-probe binding (Lee et al., 2015). Meanwhile, Sarangadharan team has studied with same EDC-NHS strategy on the Au gate for Troponin I. However, there were current increases after Troponin I antibody immobilization and current decreases after the antigen-antibody or detection binding (Sarangadharan et al., 2018).

In the transfer curve shown in Fig. S3, there are high gate leakage current and threshold voltage shift. After the DTSP treatment, the off-current increase up to 1.62 mA/mm from 0.013 mA/mm at −5 V gate voltage, leading to threshold voltage shift from −4.4 V to −5.7 V. Various studies reported that the surface charges could have induced threshold voltage shift and higher gate leakage current (Pyo et al., 2018; Kokawa et al., 2006). Therefore, Fig. S3 strongly intensify our expectation that DTSP could induce the functionalized gate surface charge and variation of surface by binding with cortisol result in cortisol sensing. Also, we expect that the chemical treatment for gate surface functionalization and antigen-antibody binding for cortisol sensing did not change the piezoelectric effect.

The off-current of the transfer curve in Fig. S3 also show same sensing result with output curve. Moreover, this result show larger detection margin compared the output curve readings among four type different cortisol concentrations.

3.2. *Optical pumping for standard cortisol sensing*

The HEMT is sensitive to light, which can lead to generate photocurrent by diverse mechanism. Here, a laser illumination or irradiation can amplify biosensor's sensitivity as reducing limit of detection (LOD). For the sensor, the laser source would illuminate the functionalized gate area fully, which was also covered with transparent PDMS on top. Since PDMS is transparent to 532 nm irradiation, the light can reach at specified area. As shown in Fig. S4, there are no absorbance at 532 nm for DTSP, c-Mab, and cortisol. Therefore, the 532 nm laser was a source only to influence the HEMT biosensor itself.

Fig. 4(a) shows the simple schematic diagram to irradiate 532 nm green laser to functionalized gate area along with its optical pumping mechanism, covering all area between source and drain for absolute coverage (Kang et al., 2015; Turkulets and Shalish, 2019). The AlGaN/GaN HEMT is a luminescence device with a direct bandgap, unlike an indirect bandgap device such as Si device. Moreover, when it was irradiated with 532 nm laser (green laser) and 623 nm laser (red laser) illumination and it was confirmed that carrier could be increased as shown in Fig. 4(b). Depending on the type of compound semiconductors, the wavelength of light can be varied, which can produces photocurrent (Buscema et al., 2015). For example, GaTe (1.7 eV bandgap), InSe (1.2 eV bandgap at bulk), and GaSe (2.1 eV bandgap) devices form largest photocurrent in the visible, visible-near infrared, UV–visible spectrum, respectively (Liu et al., 2014; Lei et al., 2014; Hu et al., 2012).

Actually, the AlGaN/GaN HEMT has been known to generate photocurrent from 650 nm (1.91 eV) to 325 nm (3.81 eV) of the UV–visible spectrum (Cheney, 2014). Considering the bandgap of GaN of 3.4 eV, electron-hole pairs are generated as carriers when irradiating light having energy higher than energy bandgap. However, when irradiating light that does not have energy above bandgap (red, green, blue light), carrier concentration also increases. In this case, the increasing rate is smaller than another case when electron-hole pair was newly generated by UV-light. Therefore, this can be explained by electron detrapping in trap inside the device. Electron trapped inside device was activated by light and join to carrier, increasing the current. Various

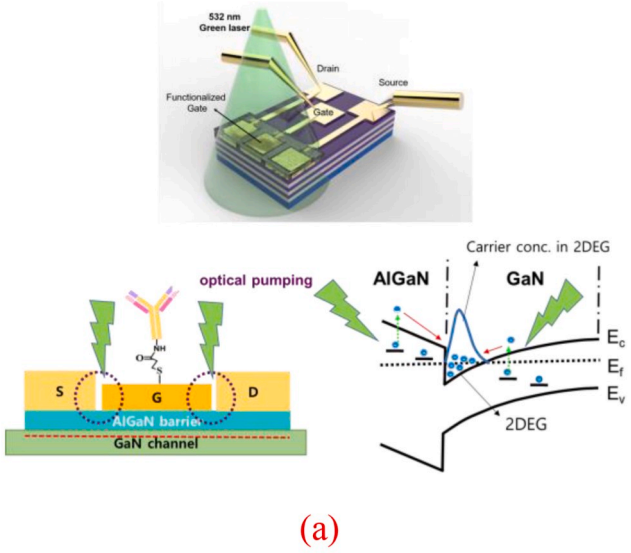

(a)

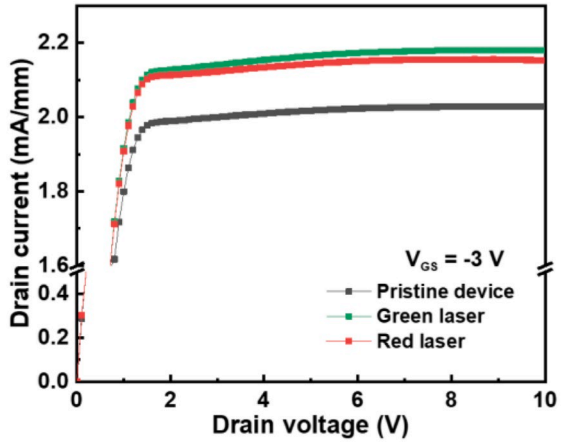

(b)

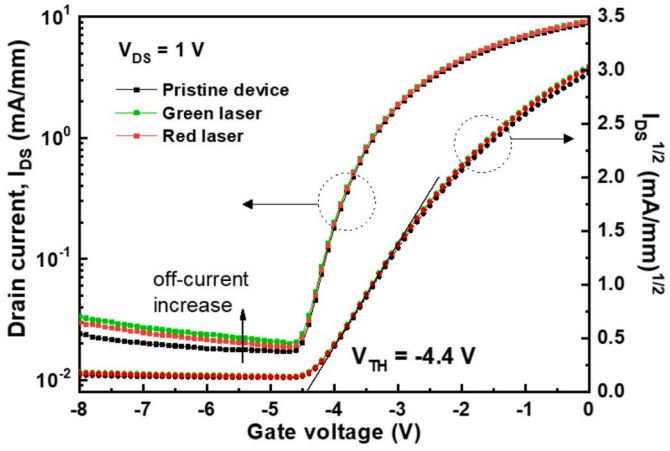

(c)

(caption on next column)

Fig. 4. (a) Schematic diagram of laser illumination to AlGaN/GaN HEMT biosensor for optical pumping along with its mechanism diagram, measured (b) output and (c) transfer characteristics of the pristine device under 532 nm laser (green laser) and 623 nm laser (red laser) illumination. Forward drain current at saturation region was increased from 2.017 mA/mm to 2.164 mA/mm at V_{DS} of 5 V and V_{GS} of −3 V due to 532 nm laser illumination in 4(b) and leakage off-current was also increased at V_{GS} of −5 V and V_{DS} of 1 V from 0.0174 mA/mm to 0.0208 mA/mm in 4(c). (For interpretation of the references to colour in this figure legend, the reader is referred to the Web version of this article.)

studies could investigate the de-trapping mechanism which was calculated by Arrhenius' equation for electron activation energy, electron recapturing energy (Kang et al., 2015, 2016).

Since 532 nm green laser energy (2.33 eV) is below the bandgap of GaN (3.4 eV), the light could not be absorbed to GaN. However, the energy is enough to activate electron trap, which would be 0.73–2.35 eV (Kang et al., 2015, 2016). Therefore, the light source was passed through junctionless gaps between gate-drain and gate-source, which was measured about 16 μm apart. Then, the light could reach AlGaN/GaN, generating photocurrent by electron de-trapping. Moreover, green laser illumination could affect to drain current at saturation region, increasing output current from 0.4659 mA to 0.4817 mA about 3.39% at −3 V gate voltage shown in Fig. S5.

As shown in Fig. S5, current increment value and ratio caused by green laser were different according to gate voltage. The increments of currents are 0.0158 mA (−3 V), 0.0385 mA (−2 V), 0.0461 mA (−1 V), 0.0558 mA (0 V), and 0.0571 mA (1 V), respectively. The bigger gate voltage becomes; the higher absolute current levels becomes. On the other hand, the increment ratio is bigger as gate voltage becomes small as shown in Fig. S5. Thus, the highest increment ratio was 3.39% at gate voltage of −3 V. Although concentration of carrier generated by optical pumping was not huge, it could be relative large percentage when original carrier concentration was low. From these results, −3 V would be a suitable gate voltage to maximize effect of the photocurrent.

Some study demonstrated that when higher gate voltage is over-driven than threshold voltage, light is emitted in the channel region. This photon energy of EL emission could have energy bandgap of 1.9–3.4 eV, which ionize the DX centers as $DX \rightarrow DX^{+} + e$. Although light emitting is going down as the HEMT is turned off, the ionized DX^{+} sometimes can survive because of large energy barrier to electron recapture. Finally, this result in persistent photoconductivity (PPC) of GaN buffer layer, leading to raise gate leakage and finally the off-state loss (Li et al., 2014). As shown in Fig. 4(c), threshold voltages (V_{TH}) in pristine device was not affected by both green and red lasers, while it augmented off-current about 19.5% by green laser compared with non-illumination condition in transfer curve. In this study, we operated the HEMT at −8 V–0 V that was not extremely high voltage to overdrive compared cases of above studies.

As compared to Fig. 3 and Fig. S6(b), HEMT biosensor output current sensing performance was enhanced with 532 nm green laser (2.33 eV) as illumination to functionalized gate area. Also, as identified in transfer curve of Fig. S6(a) and output curve of Fig. S6(b), it was demonstrated that DTSP, c-Mab for functionalization of Au thin film and cortisol were not a hindrance to carriers pumped by absorbance of light source before reaching to functionalized gate area and GaN.

Fig. 5(a) shows calculated ratios of current levels out of Fig. 3 and Fig. S6(b) output curve, which show different output current levels upon the detection of different concentrated cortisol solutions. The calculation is post-sensing cortisol (1 pM–1 nM) current value divided with pristine current ($I_{cortisol}/I_{Pristine}$) at 5 V read voltage. In case with 532 nm green laser illumination, the LOD was measured as 1 pM, where device's sensitively also could detect other cortisol concentrations, 10 pM, 100 pM, and 1 nM in sequence. On the other hand, there is no available detection based on current levels between 1 pM and 10 pM without the illumination. In a word, the illumination of 532 nm green laser enhances the sensitivity as low cortisol concentration as 1 pM and detection range

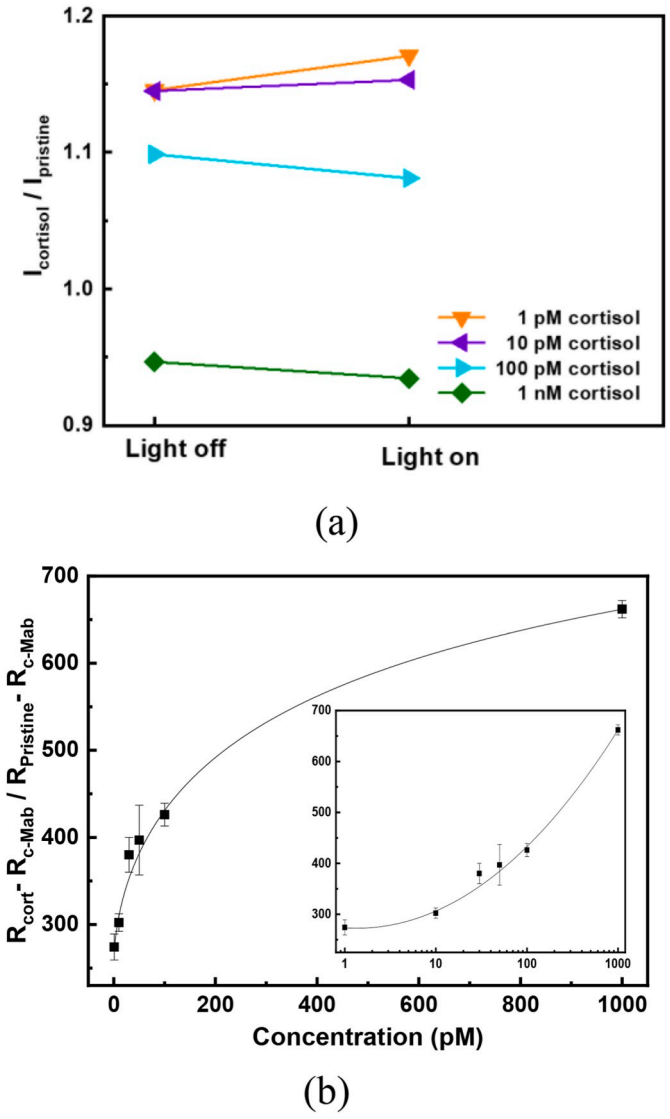

Fig. 5. (a) Calculated output current ratio as $I_{post\text{-}sensing}/I_{pristine}$ with 532 nm green laser or not after cortisol detection with standard cortisol solution 1 pM, 10 pM, 100 pM and 1 nM in a sequence. This figure shows enhanced sensitivity with 532 nm green laser, which was measured 1 pM as LOD (b) Resistance calibration plot of cortisol detection output current at 5 V from 1 pM to 1 nM and inlet graph was described as logarithmic concentration scale. (For interpretation of the references to colour in this figure legend, the reader is referred to the Web version of this article.)

covers three orders.

As remarked above, electron trap activated by green laser increase the carrier concentration, improving AlGaN/GaN HEMT biosensor sensing performance.

Experimental results with green laser illumination from −3 V to 1V of gate voltage is presented in Fig. S7, which is calculated by same method with Fig. 5(a). It also shows the best sensitivity of HEMT biosensor was with −3 V gate voltage.

Based on the current readings at gate voltage of −3 V, resistance calibration plot was available as shown in Fig. 5(b), which was obtained from R_{cort}-$R_{c\text{-}Mab}$/$R_{Pristine}$-$R_{c\text{-}Mab}$ (Kim et al., 2017). The linearity of normalized resistance calibration could demonstrate minimizing variations of sensor performances depending on the fabrication batch processes or detection protocols. And furthermore, the normalized calibration would be able to be a parameter of accurate design to be applied for a real time measurement sensing format (Kim., et al., 2017).

Even though there is a linear relationship in low concentration range by least square method, the detection ratio after 10 pM showed significant deviation out of the linearity as shown in Fig. 5(b). For the more detailed discussions, an inlet graph of Fig. 5(b) was added as logarithmic concentration scale. As shown in Fig. 5(b), a reasonable and effective detection was available from limited number of probe c-Mab molecules in constant area. It means that somehow high degree of cortisol concentration would saturate the probe molecular sites on functionalize gate, which should induce a non-linearity outcome or measurement in high cortisol concentrations. In this case, it would be better to further dilute sample for the exact detection.

3.3. 532 nm laser optical pumping for real salivary cortisol detection

Toward utilization for commercialization, the major key is using of real human sample as well as standard sample. There are diverse methods to extract real human cortisol sample from blood, urine and salivary (Kim et al., 2017; Jung et al., 2018). Among them, salivary cortisol is good choice in point of noninvasive and fast acquirement method. Furthermore, salivary cortisol is routinely used as a biomarker of psychological stress and related mental or physical diseases. Most studies consider the salivary cortisol levels as a reliable measurement marker of hypothalamus-pituitary-adrenal axis (HPAA) adaptation to stress (Hellhammer et al., 2009). The required salivary volume for detection was only 5 μL based on the PDMS microfluidic format. Therefore, it can be immediately applicable to a point-of-care test (POCT) system. Finally, the experiments were performed with real sample such as human salivary after sample dilutions.

Fig. 6(a) shows the output curve and Fig. 6(b) shows the transfer curve with the diluted salivary samples (1 × , 10 × , 100 × , and 200 ×) with 532 nm laser illumination. For comparisons, as shown in Fig. S8(a) with output and S8(b) with transfer, the identical measurements without 532 nm laser illumination were performed and illustrated. As shown in Fig. 6(b), off-currents of the transfer curve during sensing could show relatively large margins among differently salivary samples, when it is compared with the output curve margins among the same samples. In this case, the EA was used to passivate empty site, which is generated by DTSP modification without binding of antibody. Cortisol detection strategy and method is same as the process of experiment with standard cortisol solution.

Fig. S9shows selectivity test that the HEMT sensor was evaluated by comparing the relative current changes(ΔI) in response to 10 pM cortisol, cortisone, corticosterone, and progesterone, relatively. To ensure selectivity of the biosensor with other interferences, especially for the case of salivary samples, three hormones were chosen and comparatively examined. As shown in Fig. S9, there were no significant detections toward the other hormones including very close cortisol analogues, such as cortisone and corticosterone (Jo et al., 2020).

In Fig. 6(a) and (b), the biosensor could detect 200 × dilution salivary cortisol in the first time regardless of green laser optical pumping. However, 100 × dilution salivary cortisol can't be detected without 532 nm green laser. In addition, an undiluted sample (1 ×) could not be distinguishable with 10 × diluted salivary sample. On the other hand, 200 × , 100 × , 10 × and 1 × salivary cortisol solutions were well detected as different output currents with 532 nm green laser pumping as shown in Fig. 6(a). This result also stably supports that the laser optical pumping could help to enhance the HEMT biosensor accuracy as Fig. 6(c) shows calculated ratios of current levels, which again shows different output current levels upon the detection of differently diluted salivary samples as like as Fig. 5(a). Since the concentration of human salivary cortisol is known about 1–16 nM (Persson et al., 2008), it was found that the 200 × ~100 × dilution would be ideal for stable sensing.

Morning salivary cortisol concentration is known to be 10–17 ng/mL (27.6–46.9 nM), while midnight salivary cortisol concentration is about 2 ng/mL (5.5 nM) (Kim et al., 2015). Since morning salivary cortisol is thicker than midnight salivary cortisol, experimental progress was done from midnight salivary to morning salivary (Kim et al., 2017; Jung et al.,

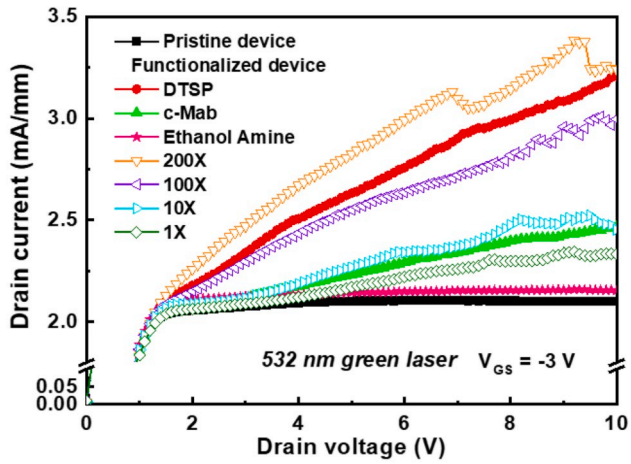

(a)

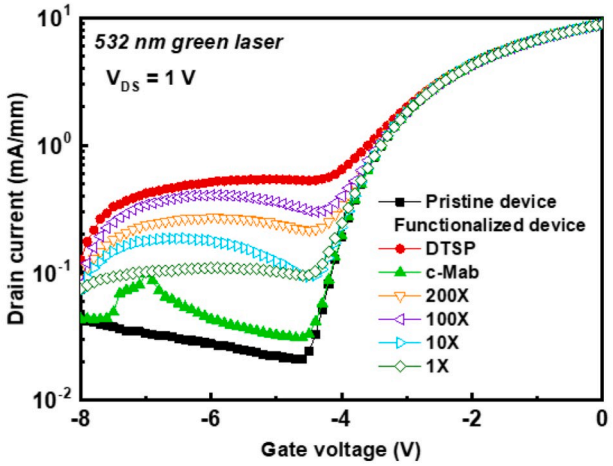

(b)

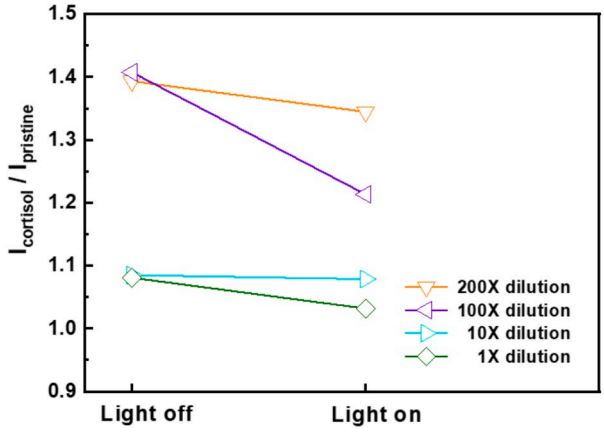

(c)

Fig. 6. (a) The output curve and (b) the transfer curve with the diluted salivary samples (1 × , 10 × , 100 × , and 200 ×) with 532 nm laser illumination (c) calculated output current ratio as $I_{post\text{-}sensing}/I_{pristine}$ with or without 532 nm green laser for cortisol detection with differently diluted human salivary samples (1 × , 10 × , 100 × , and 200 ×). (For interpretation of the references to colour in this figure legend, the reader is referred to the Web version of this article.)

2018). To compare the morning and midnight samples more intensively, measurements with or without green and red lasers were performed and compared as shown in Fig. S10. For entire cases, midnight samples showed high $I_{cortisol}/I_{pristine}$ ratios representing lower concentrations (less than 1 nM) than those of morning samples obtained by extrapolation based on the ratios in Fig. 5(a).

At 5 V for reading voltage, the current increase with DTSP and decrease with c-Mab binding was shown. Since there could be an issue of electrical double layer in physiological condition, the successful detection was meaningful. For the salivary samples in Fig. 6(a), (b), 6(c) and Fig. S10, the distinguishable results compared by standard solution experiment were increases of current caused by EA passivation. Similar to DTSP, the EA include amine group. At the same reason, it could withdraw the electron or could be positively charged in aqueous condition, raising carrier concentration. As a result, the current was higher than current of pristine device.

4. Conclusion

A cortisol biosensor using AlGaN/GaN HEMT device has been demonstrated as a FET format. The device characteristics of sensor could exhibit the LOD of 1 pM cortisol by immune-sensing of c-Mab, which was demonstrated by changes of saturated output curve and sub-bandgap current. The LOD was enhanced by illumination of the light source to increase HEMT carrier of 2DEG. Consequently, HEMT device with the green light pumping source was useful for detection enhancement of cortisol, which was also proven to be effective in actual human salivary samples. The study can extend an outreach on the development of a direct FET sensor for salivary cortisol monitoring.

Declaration of competing interest

The authors declare that they have no known competing financial interests or personal relationships that could have appeared to influence the work reported in this paper.

CRediT authorship contribution statement

Kyoungmin Woo: Writing - original draft. **Wonkyu Kang:** Methodology, Formal analysis, Software. **Kyungmin Lee:** Investigation, Methodology. **Pilwoo Lee:** Project administration. **Yoonjae Kim:** Visualization. **Tae-Sik Yoon:** Validation. **Chu-Young Cho:** Investigation, Methodology, Writing - original draft. **Kyung-Ho Park:** Supervision, Project administration. **Min-Woo Ha:** Writing - original draft, Supervision. **Hyun Ho Lee:** Conceptualization, Data curation, Formal analysis, Funding acquisition, Supervision, Project administration, Formal analysis.

Acknowledgment

This research was supported by the Pioneer Research center program through the National Research Foundation of Korea (NRF) of Republic of Korea (No. 2014M3C1A3053035) funded by the Ministry of Science, ICT and also supported by Convergent Technology R&D Program for Human Augmentation through the NRF funded by Ministry of Science and ICT (No. 2019M3C1B8077549). Authors also would like to thank to Professor Jinsung Park at Korea University in Sejong, for kind offering of cortisone, corticosterone, and progesterone for selectivity examinations.

Appendix A. Supplementary data

Supplementary data to this article can be found online at https://doi.org/10.1016/j.bios.2020.112186.

References

Ambacher, O., Smart, J., Shealy, J.R., Weimann, N.G., Chu, K., Murphy, M., Schaff, W.J., Eastman, L.F., Dimitrov, R., Witter, L., Stutzmann, M., Rieger, W., Hilsenbeck, J., 1999. J. Appl. Phys. 85, 3222–3232.

Arya, S.K., Chornohur, G., Venugopal, M., Bhansali, S., 2010a. Analyst 135, 1941–1946.

Arya, S.K., Chornohur, G., Venugopal, M., Bhansali, S., 2010b. Biosens. Bioelectron. 25, 2296–2301.

Buscema, M., Island, J.O., Groenendijk, D.J., Blanter, S.I., Steele, G.A., Zant, van der, Herre, S.J., Castellanos-Gomez, A., 2015. Chem. Soc. Rev. 44, 3691–3718.

Chen, C.-P., Ganguly, A., Lu, C.-Y., Chen, T.-Y., Kuo, C.-C., Chen, R.-S., Tu, W.-H., Fischer, W.B., Chen, K.-H., Chen, L.-C., 2011. Anal. Chem. 83, 1938–1943.

Cheney, D.J., 2014. ECS Trans. 61, 197–204.

Choi, K., Kim, J., Ahn, J., Choi, J., Im, M., Choi, Y., 2012. Lab Chip 12, 1533–1539.

Cimalla, I., Will, F., Tonisch, K., Niebelschutz, M., Cimalla, V., Lebeddev, V., Kittler, G., Himmerlich, M., Krischok, S., Schaefer, J.A., Gebinoga, M., Schober, A., Friedrich, Ambacher, O., 2007. Sensor. Actuator. B Chem. 123, 740–748.

Domes, G., Stächele, T., von Dawans, B., Heinrichs, M., 2019. Psychoneuro 105, 117–122.

Hellhammer, D.H., Wust, S., Kudielka, B.M., 2009. Psychoneuro 34, 163–171.

Horio, K., Nakajima, A., 2010. Phys. Status Solidi C 7, 1931–1933.

Hu, P., Wen, Z., Wang, L., Tan, P., Xiao, K., 2012. ACS Nano 6, 5988–5994.

Huq, H.F., Hector Trevino, I., Castillo, J., 2016. J. Mod. Phys. 7, 1712.

Jeon, J., Uthaman, S., Lee, J., Hwang, H., Kim, G., Yoo, P.J., Hammock, B.D., Kim, C.S., Park, Y.-S., Park, I.-K., 2018. Sensor. Actuator. B Chem. 266, 710–716.

Jo, S., Lee, W., Park, J., Kim, W., Kim, W., Lee, G., Lee, H.-J., Hong, J., Park, J., 2020. Sensor. Actuator. B Chem. 304, 127424.

Jung, H., Jung, J., Kim, Y.-H., Kwon, D., Kim, B.-G., Na, H.B., Lee, H.H., 2018. BioChip J. 12, 249–256.

Kang, T.-S., Ren, F., Gila, B.P., Pearton, S.J., Patrick, E., Cheney, D.J., Law, M., Zhang, M.-L., 2015. J. Vac. Sci. Technol. B 33, 061202.

Kang, T.-S., Lin, Y., Ahn, S., Ren, F., Gila, B.P., Pearton, S.J., Cheney, D.J., 2016. J. Vac. Sci. Technol. *B* 34, 011203.

Kim, K.S., Jang, J.-R., Choe, W.S., Yoo, P.J., 2015. Biosens. Bioelectron. 71, 214–221.

Kim, K.S., Lim, S.R., Kim, S.-E., Lee, J.Y., Chung, C.-H., Choe, W.S., Yoo, P.J., 2016. Sensor. Actuator. B Chem. 242, 1121–1128.

Kim, Y.-H., Kim, M., Oh, S., Jung, H., Kim, Y., Yoon, T.-S., Kim, Y.-S., Ho Lee, H., 2012. Appl. Phys. Lett. 100, 163301.

Kim, Y.-H., Lee, K., Jung, H., Kang, H.K., Jo, J., Park, I.-K., Lee, H.H., 2017. Biosens. Bioelectron. 98, 473–477.

Kokawa, T., Sato, T., Hasegawa, H., Hashizume, T., 2006. J. Vac. Sci. Technol. B 24, 1972–1976.

Lagger, P., Ostermaier, C., Pobegen, G., Pogany, D., 2012. IEDM Tech. Dig. 13, 1.1-13.1.4.

Lee, B., Heo, J.H., Lee, J.W., Cho, H.H., Lee, J.H., 2019. Sci. Adv. Mater. 11, 1699–1704.

Lee, H.H., Bae, M., Jo, S.-H., Shin, J.-K., Son, D.H., Won, C.-H., Jeong, H.-M., Lee, J.-H., Kang, S.-W., 2015. Sensors 15, 18416–18426.

Lei, S., Ge, L., Najmaei, S., George, A., Kappera, R., Lou, J., Chhowalla, M., Yamaguchi, H., Gupta, G., Vajtai, R., 2014. ACS Nano 8, 1263–1272.

Li, B., Jiang, Q., Liu, S., Liu, C., Chen, K.J., 2014. Phys. Status Solidi C 11, 928–931.

Liu, F., Shimotani, H., Shang, H., Kanagasekaran, T., Zolyomi, V., Drummond, N., Fal'ko, V.I., Tanigaki, K., 2014. ACS Nano 8, 752–760.

Neuberger, R., Muller, G., Ambacher, O., Stutzmann, M., 2001. Phys. Status Solidi 185, 85–89.

Parlak, O., Keene, S.T., Marais, A., Curto, V.F., Salleo, A., 2018. Sci. Adv. 4, eaar2904.

Pearton, S.J., Ren, F., Chu, B.H., 2013. Functionalized GaN Bsed Transistors for Biosensing, pp. 225–251.

Persson, R., Garde, A.H., Hansen, Å.M., Österberg, K., Larsson, B., Ørbæk, P., Karlson, B., 2008. Chronobiol. Int. 25, 923–937.

Pyo, J.-Y., Jeon, J.-H., Koh, Y., Cho, C.-Y., Park, H.-H., Park, K.-H., Lee, S.W., Cho, W.-J., 2018. AIP Adv. 8, 085106.

Saito, W., Kuraguchi, M., Takada, Y., Tsuda, K., Omura, I., Ogura, T., 2005. IEEE Trans. Electron. Dev. 52, 159–164.

Sarangadharan, I., Regmi, A., Chen, Y.-W., Hsu, C.-P., Chen, P.-C., Chang, W.-H., Lee, G.-Y., Chyi, J.-I., Shiesh, S.-C., Lee, G.-B., Wang, Y.L., 2018. Biosens. Bioelectron. 100, 282–289.

Shen, M., Li, B., Li, Y., 2014. Biosens. Bioelectron. 60, 101–111.

Steinhoff, G., Purrucker, O., Tanaka, M., Stutzmann, M., Eickhoff, M., 2003. Adv. Funct. Mater. 13, 841–846.

Stern, E., Klemic, J.F., Routenberg, D.A., Wyrembak, P.N., Turner-Evans, D.B., Hamilton, A.D., LaVan, D.A., Fahmy, T.M., Reed, M.A., 2007. Nature 445, 519–522.

Sun, K., Ramgir, N., Bhansali, S., 2008. Sensor. Actuator. B Chem. 133, 533–537.

Turkulets, Y., Shalish, I., 2019. Appl. Phys. Lett. 115, 023502.

Varghese, A., Periasamy, C., Bhargave, L., 2019. IEEE Sensors 18, 747–755.

Vasudev, A., Kaushik, A., Tomizawa, Y., Norena, N., Bhansali, S., 2013. Sensor. Actuator. B Chem. 182, 139–146.

Vericat, C., Vela, M., Benitez, G., Carro, P., Salvarezza, R., 2010. Chem. Soc. Rev. 39, 1805–1834.

Yang, J., Carey, P., Ren, F., Wang, Y.-L., Good, M.L., Jang, S., Mastro, M.A., Pearton, S.J., 2017. Appl. Phys. Lett. 111, 202104.